Journal of Scientific & Industrial Research
Vol. 84, November 2025, pp. 1230-1240
DOI: 10.56042/jsir.v84i11.5581

Experimental Investigations of Model-Free Control Approaches on Control of Shape Memory Alloy (SMA) Spring Actuated Parallel Manipulator

Ranjith Pillai R* & Murali Ganesan

Department of Mechatronics Engineering, College of Engineering and Technology,
SRM Institute of Science and Technology SRM Nagar, Kattankulathur, 603 203, Kanchipuram, Chennai, Tamil Nadu, India

Received 14 September 2023; revised 27 November 2025; accepted 08 December 2025

Robots in the industry are mostly used for assembly operations. Robot assembly is a difficult operation that requires additional compliance to reduce the position error between two mating parts. Flexible parallel manipulators, owing to their accuracy in positioning and inherent compliance, are suitable for use as orienting mechanisms. This paper describes a two-degree-of-freedom flexible parallel manipulator driven by Shape Memory Alloy (SMA) springs, designed to function as an auxiliary orientation unit for a tabletop Cartesian robot. While SMA springs provide advantages such as compact integration, simple actuation, and high power density, their nonlinear characteristics significantly increase the complexity of the control process. Apart from handling nonlinearities and disturbances, the controller should be capable of controlling the co-contraction of actuators in the mechanism. Model-free Sliding Mode Control (SMC) with linear and nonlinear sliding surfaces is chosen for the servo control, combined with the Time Delay-based Estimation (TDE) as a secondary control for the implementation and performance analysis. This study presents an experimental comparison of nonlinear control strategies for trajectory tracking in the developed redundant parallel manipulator. Efficient Trajectory tracking characteristics are crucial for any motion platform, and hence, real-time experiments with complex trajectories are conducted on the prototype in the presence of external disturbances, and the results of the experimentation are presented, which demonstrate the superior nature of nonlinear SMC over other controllers. The inclusion of the secondary term (TDE) in the design of control is found to linearize the closed-loop system.

Keywords: Flexible parallel manipulator, Motion Platform, Redundant parallel manipulator, Robot assembly, Servo control

Introduction

Parallel manipulators belong to a class of robotic systems characterized by closed-chain kinematics, typically consisting of a stationary base and a mobile platform connected through multiple limbs or actuators. These architectures are widely selected for motion-tracking applications and simulation tasks due to their comparatively high precision, accuracy, load-carrying capability, and structural stiffness.[1–3] However, they also present notable drawbacks, including limited workspace, challenging forward-kinematic analysis, and strongly coupled nonlinear dynamics, all of which complicate parameter identification and make control design more demanding.[4] Parallel robots are the best choice for applications like precise machining, drilling, material handling, robot wrist for assembly, and surgical robots that require limited motion but high accuracy. Parallel robotic architectures allow the integration of non-traditional actuators, including smart materials, thereby opening new research directions. These unconventional actuators facilitate the development of compact and compliant parallel mechanisms suitable for operation in unstructured environments while offering improved positioning capability. Although their inclusion adds complexity to the system dynamics and control design, it enables significant miniaturization. Among such smart materials, SMA are widely used in miniature systems because of their low weight, ease of integration, simple actuation, silent operation, and high power density.[5] SMAs, typically composed of Nickel–Titanium (NiTi), recover a predetermined shape or length when thermally activated. This shape memory effect arises from a phase transformation between low-temperature marten site and high-temperature austenite during heating. However, SMA actuators exhibit hysteresis, causing response delays and motion inaccuracies, making their control an important and ongoing research challenge. A wide range of studies have demonstrated the integration of SMA actuators in parallel robotic systems. Notable examples include a Stewart platform driven by SMA wires[6], a parallel mechanism incorporating a novel strain-amplification approach for

*Author for Correspondence
E-mail: ranjithr1@srmist.edu.in

SMA elements[7], and a two-degree-of-freedom joint realized through three SMA wires.[8] Other developments feature a ball-and-beam stabilizing setup employing two SMA wires in an antagonistic layout[9–11], as well as a recent modular parallel "flexibot" that utilizes SMA springs as its actuation scheme.[12] Shape Memory Alloy springs can be used as an alternative to the wires for high strain, but suffer from slow response, high inductive nature and control complexity. Extensive research has focused on the motion-tracking control of SMA actuators. Achieving accurate tracking is challenging because SMAs exhibit strong nonlinearities, and the control strategy must adequately address their hysteresis behaviour. Various control laws have been introduced, often incorporating hysteresis models such as the Preisach formulation[13–15], the Liang model[16], or the Duhem representation[17], and combining them with feedback schemes like PID or sliding-mode control. These methods, however, rely heavily on precise SMA modelling, which is difficult to obtain due to the actuator's nonlinear characteristics. In addition, several well-known servo-control approaches reported in the literature include sliding-mode, fuzzy-logic, and adaptive control techniques.[9–11,18–22] Due to the uncertainty in model prediction and to reduce complexity in hardware implementation, our objective is to have a model-free control approach for an SMA spring actuator with hysteresis compensation. On studying the literature pertaining to model-free control approaches, Time delay-based estimation techniques are a popular model-free technique used by many researchers in control to compensate for nonlinearities and uncertainties in the dynamics of the system.[23–29] It is important to note that existing control strategies have predominantly addressed SMA wire actuation in antagonistic configurations. This motivated the need to examine how nonlinear controllers perform when applied specifically to SMA springs integrated within a parallel mechanism, thereby allowing assessment of their capability to handle actuator co contraction, coupling effects, and structural uncertainties.

The key contributions of this study are outlined below. A comparative study of model-free Sliding mode control with linear and nonlinear sliding surface, along with TDE and PID control, is conducted experimentally on the 2 Degree of Freedom (DoF) redundant parallel robot through various test scenarios. A symmetric parallel manipulator has been developed in the laboratory using the minimum number of actuators required for its motion, with the intention of employing it as a wrist-type orientation mechanism, as shown in Fig. 1. Reducing the actuator count lowers both power requirements and controller workload. The paper provides a comprehensive mathematical formulation covering the kinematic model, differential kinematics, singularity evaluation, and dynamic analysis. The results show that the manipulator operates without singularities throughout its intended workspace. The choice of SMC as a servo is motivated by its ability to handle non-linearities and parameter uncertainties.[30,31] The TDE technique, which estimates the unknown dynamics and disturbances online through input-output data, is also combined with the control loop and tested for the SMA spring actuator. The nonlinear SMC is expected to perform better in the trajectory tracking due to its ability to handle nonlinearity better and avoid velocity saturation problems, unlike linear SMC. The experimental result on the robot verifies the same.

System Design and Mathematical Description

In this section, the experimental setup is explained, and the mathematical description is also briefly addressed. The mathematical description involves the inverse kinematic model of the platform and a general dynamic model, which is used in the design of TDE-based controllers.

System Design

The experimental platform consists of a symmetric spatial parallel manipulator driven by SMA springs. Although spatial parallel mechanisms typically provide six degrees of freedom, the system used in this work achieves only two—roll and pitch—because a universal joint is incorporated between the top moving plate and the center of the fixed base. Both the base and the end-effector plates have triangular

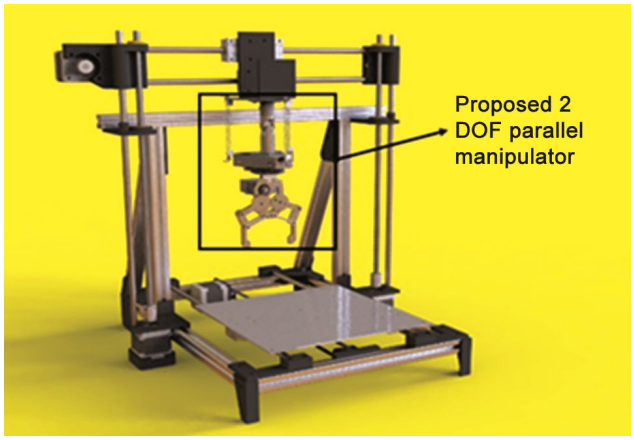

Fig. 1 — Proposed application

geometries, and electrically conductive pin joints are mounted at their vertices to accommodate the SMA spring actuators. The dimensions of the upper and lower plates are kept identical to minimize actuator coupling effects.[32] The actuation is provided by a one-way NiTi spring procured from Dynalloy. Bidirectional motion is obtained by co-contracting opposing actuator pairs arranged symmetrically. The specifications of the SMA springs and the robotic structure are given in Table 1, while Fig. 2(a) illustrates the conceptual CAD model of the manipulator.

The experimental arrangement incorporates all supporting hardware, including sensors, driver circuits, data-acquisition units, and control modules required for motion regulation. A 6-axis Inertial Measurement Unit (IMU), MPU6050, is fixed at the center of the end-effector plate to record its orientation. In this study, the SMA spring displacement is not measured directly; instead, it is estimated using the robot's kinematic model, with IMU-derived orientation as input. A direct measurement approach—using an external camera together with end-effector orientation data to track the distance between two white markers attached to the spring ends—was initially considered. However, the indirect method was selected because achieving the 1 ms update rate required by the control loop was not feasible with the camera hardware. Three LTS6NP current sensors are incorporated to monitor the actuation currents of the SMA elements. The SMA drivers are powered by a KEYSIGHT triple-output DC supply (0–30 V, 5 A). Data are acquired through a National Instruments cDAQ platform equipped with an Analog input and output module, while IMU readings are transferred via serial communication from an Arduino Mega. The control scheme is implemented in MATLAB/Simulink and executed on a workstation running an Intel Xeon 64-bit processor at 2.2 GHz with 24 GB of RAM. Additional details of the prototype can be found in the work of Pillai *et al.*[35,36]

Inverse Kinematic Model

The inverse kinematics of the parallel manipulator determines the required actuator lengths for a specified end-effector orientation. The geometric representation of the mechanism, including the coordinate frames and vectors used in deriving the kinematic model and Jacobian, is illustrated in Fig.2(b). The geometric quantities are defined as follows: the base frame {B}, with axes $X_B Y_B Z_B$, is positioned at the centroid of the base plate; the universal joint frames $J_{1,2}$, with rotation

Table 1 — Specifications of the parallel manipulator and the actuator

Part	Material	Specification
Top (end effector) and base plate	Acrylic	100 mm (Side); 4.0 mm (Width)
Universal joint	Alloy steel	84 grams (wt.); 76 mm (Height)
Manipulator prototype		260 grams (Weight) ; 88 mm (Height)
SMA actuator (spring)	Nickel titanium (by muscle wire)	Wire Diameter: 0.75 mm Diameter of spring -6.0 mm Current limit- 3 A (maximum) Force limit- 6 N (maximum) Contraction limit -3 cm (maximum) Deformation limit-14 cm (maximum)

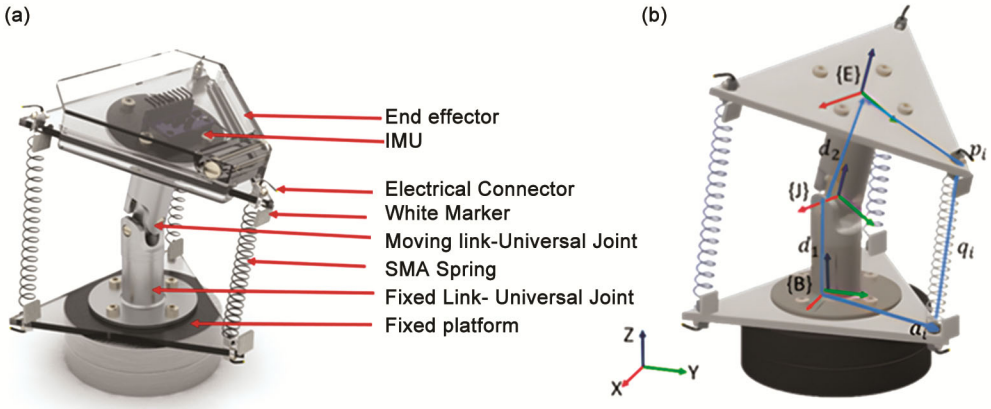

Fig. 2 — (a) Parallel Manipulator model (b) Frame assignment in the manipulator

axes X_j, Y_j, are located at the centers of the respective moving links; and the end-effector frame {E}, with axes $X_E Y_E Z_E$, is placed at the centroid of the moving platform. The points $p_i$and $a_i$denote the actuator attachment locations on the end effector and base plate, with their position vectors expressed as $P_i$in frame {E} and $A_i$in frame {B}. The vector $q_i$represents the displacement of i-th actuator, with unit direction vector S_i. The vectors $d_1$and $d_2$correspond to the passive limb length and the moving limb length, expressed in frames {B} and $J_{1,2}$, respectively.The vector loop equation can be written as (from Fig. 2(b))

$$l_i = q_i s_i = d^B + R_E^B P_i^E - A_i \quad \ldots (1)$$

where, l_i is the length of the ith actuator, d^Bdenotes the position of origin of end effector frame {E} with respect to {B} as given in Eq. (2), R_M^B describes the orientation of the end effector with respect to the base, as given in Eq. (3).[33]

$$d^B = [\mathrm{S}\,\theta_y\,\mathrm{C}\,\theta_x d_2\,, -\mathrm{S}\,\theta_x d_2\,, d_1 + d_2\,\mathrm{C}\,\theta_x\,\mathrm{C}\,\theta_y]^T \quad \ldots (2)$$

$$R_E^B = \begin{bmatrix} \mathrm{C}\,\theta_y & \mathrm{S}\,\theta_x\,\mathrm{S}\,\theta_y & \mathrm{S}\,\theta_y\,\mathrm{C}\,\theta_x \\ 0 & \mathrm{C}\,\theta_x & -\mathrm{S}\,\theta_x \\ -\mathrm{S}\,\theta_y & \mathrm{C}\,\theta_y\,\mathrm{S}\,\theta_x & \mathrm{C}\,\theta_x\,\mathrm{C}\,\theta_y \end{bmatrix} \quad \ldots (3)$$

P_i^E and A_i denotes the actuator attachment locations at the end effector and base, which can be computed based on the geometry.The actuator displacement is calculated as in Eq. (4)

$$l_i^T l_i = q_i^2 = [d^B + R_E^B P_i^E - A_i]^T [d^B + R_E^B P_i^E - A_i] \quad \ldots (4)$$

The manipulator's work envelope for the defined range of motion $-15^{\circ} \le \theta_1, \theta_2 \le 15^{\circ}$ is shown in Fig. 3.

The differential kinematic model and the singularity analysis are derived by Pillai *et al.*[35,36] based on the work of Gosselin *et al.*[34]

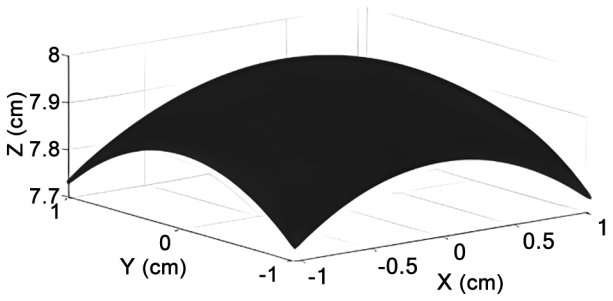

Fig. 3 — Work Envelope of the proposed manipulator

Dynamic Model

The description of the dynamics of the proto-0typeincludesthe dynamics of the SMA spring actuator and upper plate. The manipulator dynamics can be described in general as in Eq. (5).[12,29]

$$I(q)\ddot{q} + C(q,\dot{q}) + G(q) + B\dot{q} + d = h_i(q,\dot{q},f_a) + f_{ai} \times r \quad \ldots (5)$$

where, $I(q)$ is the top plate inertia, including joint mass,$q = [l_1, l_2, l_3]$ represents SMA spring displacement, as in, $C(q,\dot{q})$ denotes the vector of nonlinear dynamic effects, including centrifugal and coriolis terms. $B(\dot{q})$ describes the manipulator's frictional forces, while $G(q)$ represents the gravity-induced vector. The disturbance vector d accounts for both internal effects – such as unmodeled dynamics and actuator parameter variations—and external influences arising from payload changes and interactions with the environment. The $h_i(q,\dot{q},f_a)$ characterizes the nonlinear hysteresis behaviour. The control input vector $f_{ai} = [f_1, f_2, f_3]$ corresponds to the applied force by the SMA spring actuators. Each actuator force can be expressed as $f_{ai} = \alpha_i u_i$ where, α_i and u_i are the input coefficient and the applied current.

In the above equation, estimating the value of friction B, hysteresis term $h_i(q,\dot{q},f_a)$ is difficult as they are subjected to uncertainties. To note that this work has not estimated any dynamic parameters rather has used the dynamic equation to formulate and explain the control law. The dynamic equation can be rewritten using a constant diagonal matrix M_i as in Eq. (6).

$$M_i\ddot{q} + h = u_i \quad \ldots (6)$$

where,

$$h = \left(\frac{I(q)}{\alpha_i} - M\right)\ddot{q} + \frac{1}{\alpha_i}(C(q,\dot{q}) + G(q) + B(\dot{q}) + d - h(q,\dot{q},f_a))$$

In the above Eq. (6), h is the total non-linearities, including hysteresis, dynamic uncertainties and external disturbance whose value is unknown but bounded.

Controller Description

The inclusion of the SMA spring as an actuator brings in control challenges because of its nonlinear behaviour, high response time due to inductive effect and hysteresis.The dynamics of shape memory alloy vary with their fabrication process, environmental conditions (temperature dependence), ageing, etc, which makes the

prediction of the model very difficult due to the parameter uncertainties.[12] Many control strategies are developed to compensate for the nonlinear effects like hysteresis using mathematical models, but are found to be very complex to estimate the parameters and to implement. From an application point of view, less complex and directly implementable with intuitive gain tuning, like controllers, are preferred, which motivated us to look for model-free nonlinear controllers. Understanding the need to compensate for the nonlinear effects for better tracking control, the choice of a partition-based control law is preferred in this work. The partitioned control strategy consists of two components: a primary servo controller responsible for tracking the position error, and a secondary controller that compensates for hysteresis and other nonlinear effects. The secondary control action in SMA systems is intended to counteract nonlinear hysteresis, which is commonly addressed using inverse hysteresis models such as the Duhem, Liang, or empirical formulations. To avoid reliance on these complex models—which require difficult-to-estimate SMA parameters—aTDE approach is incorporated alongside the servo control.

Controller Structure

The complete control law based on the dynamic formulation as in Eq. (7) is chosen as

$$U_i = \widetilde{M}_i \gamma_i + \widehat{h_i} \quad \ldots (7)$$

where, $\widehat{h_i}$ denotes the estimated value of $h_i(q, \dot{q}, f_a)$ and γ_i denotes the servo part of the control.

The value of $\widehat{h_i}$ is estimated using TDE in this work[23–29], which does not involve any complex model. In TDE,it is assumed that $\widehat{h_i}$ at any instant, corresponds to an earlier value of the same quantity after a small delay, mathematically represented as

$$\hat{h}_i(t) = \hat{h}_i(t - T) \quad \ldots (8)$$

where, T defines the time delay or simply the sampling time of the controller as used in this work. For an SMA spring kind of a system, which is dynamically slow due to its temperature and inductive characteristics, the TDE assumption holds good. The choice of sampling time is very important for the accurate estimation of the nonlinear terms. For a sample time of 0.01s, the estimation error is considered to be negligible.[24] Therefore, the value of $\hat{h}_i(t - T)$ can be estimated from Eq. (9) as

$$\hat{h}_i(t - T) = U_i(t - T) - \widetilde{M}_i \ddot{l}_i(t - T) \quad \ldots (9)$$

Combining Eq. (7) and Eq. (9), the final control law can be written as

$$U_i(t) = \widetilde{M}_i(\gamma_i) + U_i(t - T) - \widetilde{M}_i \ddot{q}_i(t - T) \quad \ldots (10)$$

The servo control used in the work is explained below.

Servo Control

Sliding mode control is a popular control strategy to deal with parameter variation, nonlinearities and external disturbances in a plant. There are many applications of Sliding Mode Control (SMC) available in literature[11,18,20,21,27–29] for SMA, especially wires, but most are dependent on the mathematical model for control parameter tuning. There is a need to evaluate the performance of SMC when applied to SMA springs. SMC with linear and nonlinear sliding surface is chosen as the servo control for the study based on the work of Maolin Jin *et al.*[26] and Jinoh Lee *et al.*[29] The Linear and nonlinear SMC are described in Eq.(11) and Eq. (12), respectively. The detailed stability proof of the controllers can be found in the literature.[26,29]

$$\gamma_i = \ddot{q}_d + 2\lambda \dot{e} + \lambda^2 e \quad \ldots (11)$$

$$\gamma_i = \ddot{q}_d + \left(\lambda_1 \frac{k}{\cosh^2(ke)} + \lambda_2\right)\dot{e} + \lambda_1 \lambda_2 \tanh(ke) \quad \ldots (12)$$

In the above Eq. (11), λ is a design parameter which defines the slope of the sliding surface, and in Eq. (12), λ_1 defines the velocity limit of the actuator, λ_2 and k defines the dynamics of the reaching and sliding phase, respectively.

Conventional industrial PID control, as given in Eq. (13), popular for its simplicity and model-free characteristics, is also implemented and compared for performance.

$$U_i(t) = K_p e(t) + K_I \int_0^t e(t)dt + K_d \dot{e}(t) \quad \ldots (13)$$

Experimentation and Results

Real-time validation was conducted on the two DoF parallel manipulator developed in the Motion Analysis Laboratory at SRMIST, Chennai (Fig. 4). These experiments aimed to assess and compare the trajectory-tracking capabilities of the three control strategies under multiple input conditions, with and without external disturbances. The test scenarios included step inputs, sinusoidal references, and a smooth circular path of the end-effector center, enabling evaluation of tracking performance, disturbance rejection, and mitigation of cross-axis

coupling. Tracking accuracy was quantified using the Root Mean Square Error (RMSE) and Average Error (AE) metrics, as in Eq. (14).

$$RMSE = \sqrt{\frac{\sum_i^N (\theta_{di} - \theta_{ai})^2}{N}} \quad \ldots (14)$$

where, N define samples, θ_{di} and θ_{ai} define the desired and actual value of the i[th] sampling point, respectively.

Controller Setting and Implementation

The control scheme is implemented in MATLAB/Simulink and executed on a workstation interfaced with an NI cDAQ four-slot chassis equipped with a National Instruments 9264 (Analog Output) and 9219 (Analog Input) module. The NI 9264 module delivers the Simulink-generated control commands to the current driver, which actuates the SMA springs. To avoid contact-based position sensing—unsuitable due to actuator compliance—the end-effect or IMU is interfaced through an Arduino via serial communication, and its orientation data are used in the kinematic model to estimate spring displacement. Since the SMA springs employed are unidirectional, negative position errors are corrected by driving the antagonistic spring, resulting in only positive control effort being applied to each actuator. A sampling interval of 1 ms is adopted to facilitate accurate estimation of nonlinearities through TDE.[23,24] Proper implementation of mapping and saturation functions is required to prevent excessive accumulation of control effort due to the infinite loop gain inherent to TDE. For safety, the SMA actuation current is limited to a maximum of 2.5 A. The controller structure also requires the spring acceleration, which is obtained through numerical differentiation of the estimated position, as expressed in Eq. (15).

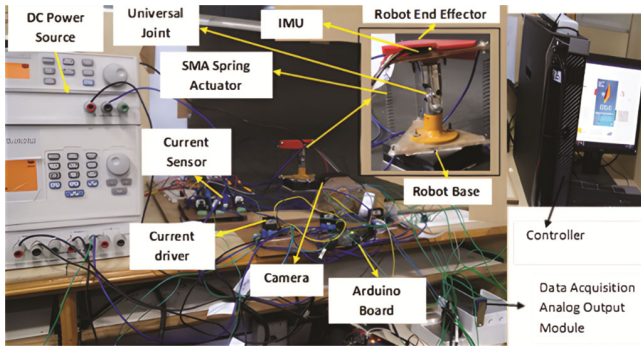

Fig. 4 — Experimental Robot prototype along with hardware set-up

$$\ddot{q}_{(t-T)} = \left(q_t - 2q_{(t-T)} + q_{(t-2T)}\right) \Big/ T^2 \quad \ldots (15)$$

where, T is the sample time

As the acceleration data is prone to noise, the use of a low-pass filter is necessary. The low value of $\widetilde{M}_i$ which is the only tuning parameter for both the controller equation, acts as the low-pass filter here.[29] The parameter $\widetilde{M}_i$ is tuned experimentally, beginning from a small initial value and incrementally increasing it until satisfactory trajectory tracking performance is obtained. The overall control framework is illustrated in Fig. 5. The PID gains are tuned experimentally by the trial-and-error method to achieve the best trajectory tracking characteristics. The other control design parameters are tuned experimentally, whose value and the effects on the output is given in Table 2.

Step Response Tracking Performance

A step input is useful for examining how the closed-loop system responds to an abrupt transition between two predefined reference values. In this

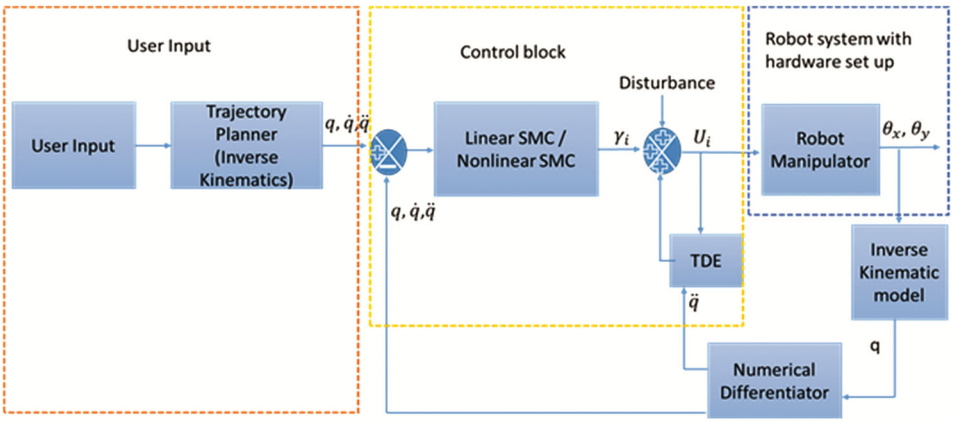

Fig. 5 — Implemented control architecture

Table 2 — Controller gains

Controller	Controller parameter	Comments
Linear SMC	λ=10	λ -Design value for slope of sliding surface.
	$\widetilde{M}_i$=0.25	High value will lead to overshoot and oscillations $\widetilde{M}_i$-Low value to act as low pass filter. Decide the responsiveness to the input. Higher value may lead to chattering effect
Nonlinear SMC	λ_1 =12	λ_1-Design parameter to limit the velocity of actuator
	k=2	k- Dynamics of sliding phase. Decides the fast convergence
	λ_2=12	λ_2- Dynamics of reaching phase. High value may lead to overshoot
	$\widetilde{M}_i$=0.1	$\widetilde{M}_i$ - Low value to act as low pass filter. Decide the responsiveness to the input
PID	K_p=12	K_p- Improves rise time
	K_I=0.6	K_I - Improves steady state error. High value can lead to overshoot
	K_D =0.01	K_D- Decreases overshoot

work, the step input is used to study the coupling effects between the robot's axes when one axis undergoes a sudden change. Specifically, one axis is commanded to move from 0° to 10° at 2 seconds, while the second axis is held at a constant 0° throughout the experiment. The dynamic step response for the X axis is shown in Fig. 6(a). From the step response plot, the rise time is found to be 2.643 sec for the Linear SMC, 2.688 sec for Nonlinear SMC and 2.506 sec for PID control. The PID control has considerable overshoot compared to the other two controllers, which settle around 2.8 sec. The intention of this experiment is to evaluate the cross-axis error rejection when one of the axes is subjected to a sudden disturbance. It is evident from Fig. 6(b) that the nonlinear SMC has shown better performance in minimizing the cross-axis error compared to the other two controllers. The Maximum error (ME) for nonlinear SMC is 0.32 degrees compared to 0.51 degrees and 1.4 degrees for Linear SMC and PID control. PID control failed to minimize the coupling effect, which is vital for the trajectory tracking of the proposed manipulator.

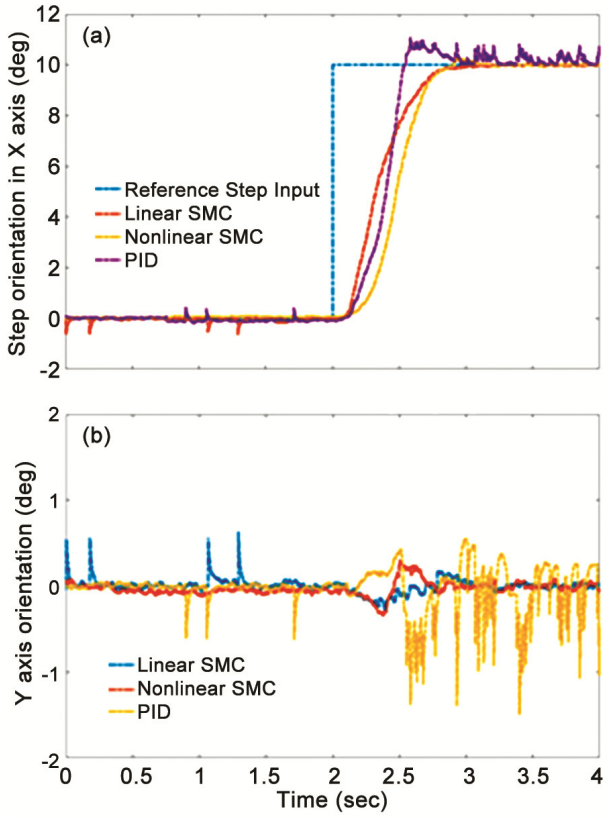

Fig. 6 — (a) Step response plot about X axis (b) Cross-axis orientation (Y axis) during step trajectory about X axis

Sinusoidal Signal Tracking Performance

A sinusoidal reference signal of 10° amplitude was applied separately to each robot axis at frequencies of 0.05 Hz, 0.1 Hz, and 0.2 Hz. This experiment evaluates the system's behaviour over different frequency conditions and offers insight into the achievable bandwidth. It also facilitates fine adjustment of the individual actuators to obtain comparable tracking performance on both axes. For input frequencies above 0.2 Hz, all controllers showed reduced accuracy, largely due to insufficient cooling of the SMA springs, which led to increased stiffness under repeated cycling. The corresponding system responses for both X and Y axes are illustrated in Figs 7(a–d), and the RMSE and AE metrics summarizing tracking performance are reported in Table 3. The results indicate that the nonlinear SMC achieved the lowest tracking error for all three input frequencies on both axes. The RMSE, as well as AE, was found to be large for frequency 0.2 Hz for all the controllers. This is because of the initial poor tracking due to insufficient heating time for the SMA spring. Therefore, it is also found that preheating the SMA spring improved the initial tracking characteristics for higher frequency input, thereby improving the bandwidth of operation.

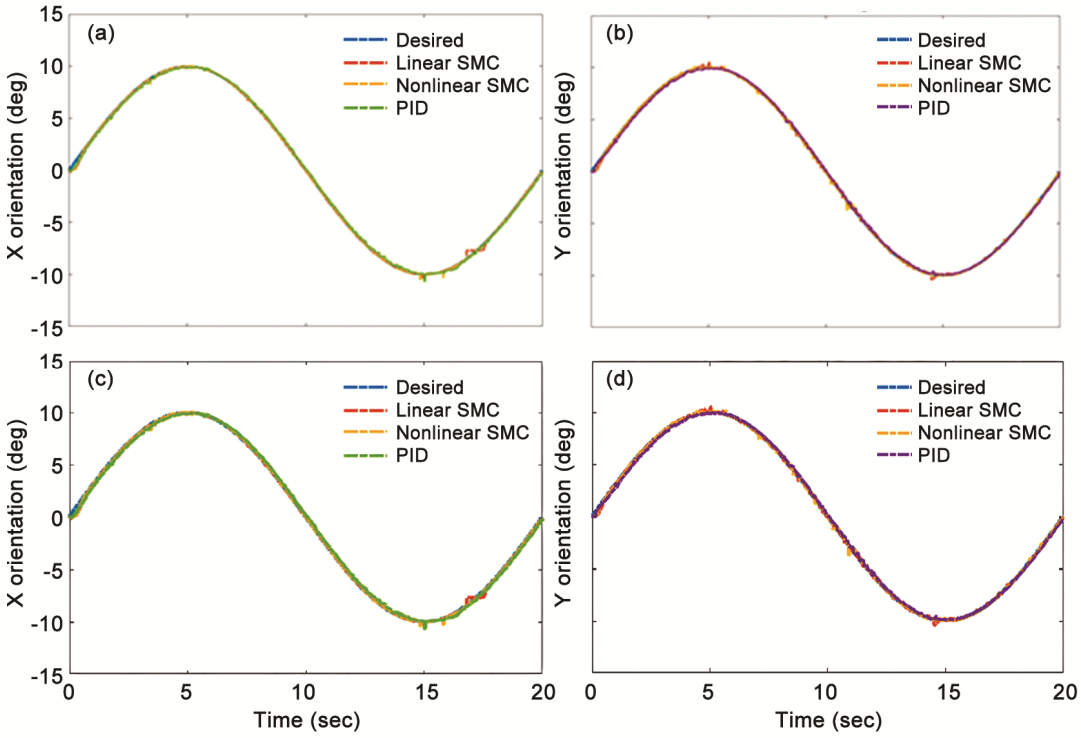

Fig. 7 — Sinusoidal trajectory response plot at various frequencies (a) X orientation response at 0.2 Hz, (b) Y orientation response at 0.20 Hz, (c) X orientation response at 0.01 Hz, (d) Y orientation response at 0.01 Hz

Table 3 — Quantitative analysis for trajectory tracking

Control Scheme	Frequency	X Orientation		Y Orientation	
		RMSE	AE	RMSE	AE
Linear SMC	Sinsoidal trajectory at 0.2 Hz	0.7147	0.19	0.4597	0.11
Nonlinear SMC		0.6813	0.18	0.3464	0.02
PID		0.8332	0.23	0.5500	0.12
Linear SMC	Sinsoidal trajectory at 0.1 Hz	0.2760	0.04	0.2428	0.01
Nonlinear SMC		0.2241	0.01	0.2138	0.01
PID		0.3132	0.06	0.3412	0.04
Linear SMC	Sinsoidal trajectory at 0.01 Hz	0.1501	0.02	0.1344	0.01
Nonlinear SMC		0.1211	0.02	0.1006	0.003
PID		0.2033	0.03	0.2140	0.03
Linear SMC	Dual Axis Sinusoidal Trajectory Tracking	0.3524	0.10	0.2228	0.01
Nonlinear SMC		0.2422	0.07	0.1485	0.01
PID		0.5147	0.33	0.4146	0.26

Dual Axis Sinusoidal Trajectory Tracking with Payload

The parallel mechanism is driven to follow sinusoidal commands on the two axes with a 90° phase shift, generating a circular path of the end effector, as illustrated in Fig. 8(a). The circle is centred at the end-effector origin, with both orientation angles initially set to zero. Circular tracking is used to assess the robot's orientation precision and its ability to maintain coordinated, smooth motion across both axes. The evaluation is carried out under two conditions: without disturbances and with disturbances. Disturbances are introduced by attaching an external payload and by operating the setup at a temperature lower than ambient using an air-conditioning system, as SMA performance is temperature-dependent. Although the mechanism is intended for light-duty tasks (≤100 g), an off-centre mass of 150 g is applied at 7.4 seconds—coinciding with the Y-axis passing through zero—to impose a significant perturbation on the end effector.

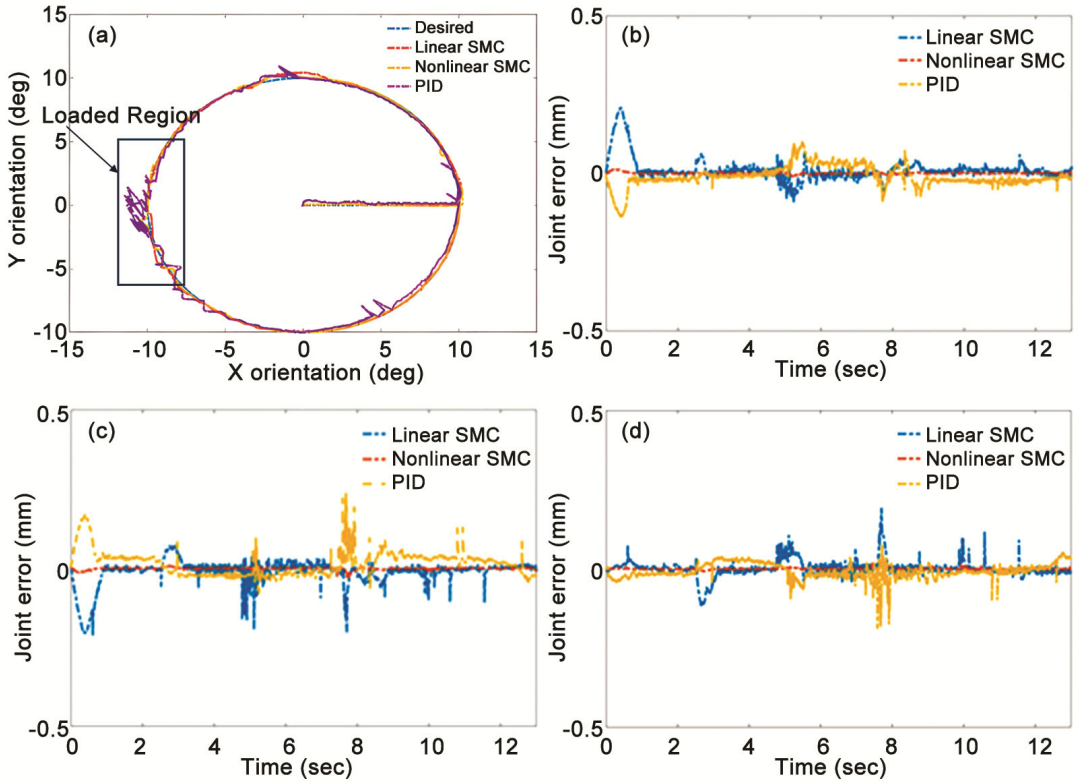

Fig. 8 — (a) Dual-axis end effector trajectory tracking response with disturbance; (b), (c), (d) Joint position error during the trajectory tracking for joint 1, 2 & 3 respectively

The responses of the three controllers during circular tracking are presented in Fig. 8(a). Nonlinear SMC provides the smoothest and most accurate trajectory in both disturbed and undisturbed cases. During the initial segment without load, PID and linear SMC exhibit oscillations near the axis crossover at approximately 5 seconds, whereas nonlinear SMC maintains a smoother path with minimal fluctuations. The imposed disturbance at 7.4 seconds generates notable oscillations, particularly for PID, leading to degraded performance. Both linear and nonlinear SMC manage the disturbance more effectively and return to the desired trajectory quickly. The joint-space tracking errors are illustrated in Figs 8(b–d), where nonlinear SMC achieves the smallest error bounds. Its RMSE and AE values are 0.2422 and 0.07 for the X-axis, and 0.1485 and 0.01 for the Y-axis, outperforming the other methods. The task-space orientation errors for the circular path are shown in Fig 9. All controllers experience higher errors in Regions 1 and 2. The increased error in Region 1 arises from the delay in reaching the SMA activation temperature, influenced by the system's thermal dynamics and the deliberately lowered ambient temperature used to emulate thermal disturbances. The summary of the responses for all the trajectories is given in Table 3.

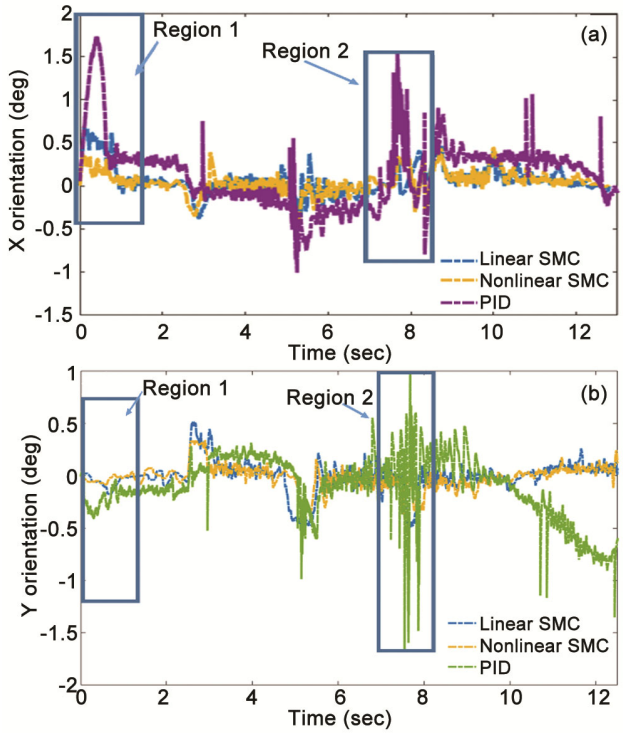

Fig. 9 — (a) X-axis orientation error during the tracking (b) Y-axis orientation error during the tracking

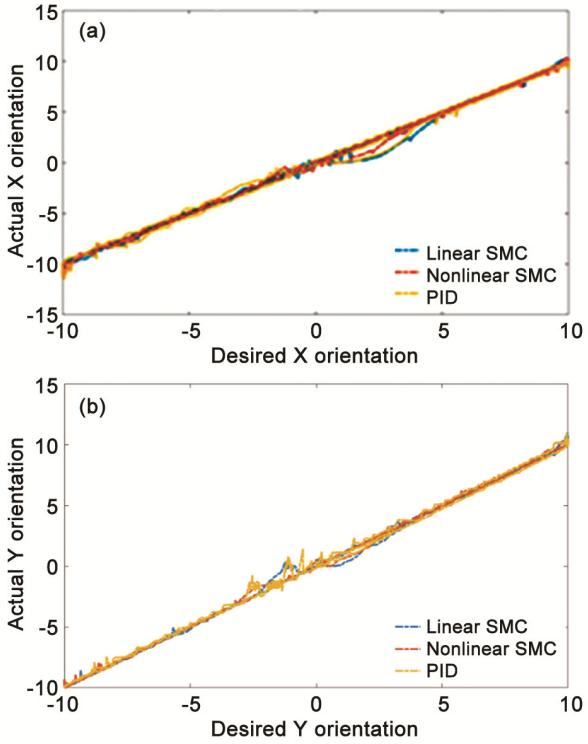

Fig. 10 — Hysteresis response curve during the dual-axis trajectory tracking: (a) About X axis, (b) About Y axis

Therefore, preheating of SMA springs can minimize the error in Region 1. The error in Region 2 above 7.4 sec is due to the sudden addition of payload. In both regions, the PID controller exhibited a very poor response compared to the nonlinear and linear SMC. The linear SMC is found to have high switching oscillations in the control input more than the nonlinear SMC due to the chattering, which could have led to poorer performance than the nonlinear SMC. The errors in the tracking also depend on the symmetry of the actuator arrangement, structural joint coupling error. The symmetrical arrangement of actuators helps in the cocontraction of antagonistic actuators and reduces stress among actuators due to the coupling forces. Therefore, the results have shown the possibility of using 3 SMA actuators in symmetry to design a manipulator rather than four with a square plate arrangement, which has reduced the controller effort. In addition, the hysterisis plot is shown in Fig. 10. The nonlinear SMC, along with TDE, almost linearizes the system and was capable of compensating for the nonlinear effect through the use of TDE.

Based on the obtained results, the following conclusions can be drawn.

(i) The mathematical description of the redundant robot is studied

(ii) Both linear and nonlinear SMC performed better in the individual axis tracking for the SMA springs in the parallel manipulator compared to the PID controller. But nonlinear SMC proved superior to linear SMC in terms of cross-axis error compensation and disturbance compensation, which is very important for the end effector tracking

(iii) The trajectory tracking results have shown the possibility of designing of manipulator using only 3 SMA actuators in symmetry with less coupling effects and good tracking characteristics.

(iv) Preheating of the SMA spring helps in improving the bandwidth and the initial tracking error in the high-frequency signal tracking

(v) The implementation of TDE, along with servo control, was able to compensate for the nonlinear hysteretic effect of SMA springs

Conclusions

In this paper, the effect of different types of controllers in improving the position tracking of SMA springs coupled to the 2 DoF parallel robot is studied experimentally. The mathematical description of the redundant robot is also briefed in the paper. The universal joint coupling, symmetrical arrangement of the actuator, influences the trajectory characteristics of the proposed robot with SMA springs. The choice of a model-free controller was made for the experimental study because of SMA modelling challenges due to nonlinearity. Real-time experiments were conducted, and the results demonstrated the efficiency of nonlinear SMC in the position control of SMA springs, leading to better trajectory tracking of the end effector with minimal cross-axis and disturbance effects. The advantage of model model-free structure and intuitive gain tuning makes the controller easily implementable for highly nonlinear systems like SMA springs. The proposed parallel robot is designed to be used as an additional wrist mechanism for orienting applications. The proposed parallel manipulator can be an excellent test bed for testing various other control schemes.

References

1 Merlet J P, *Parallel Robots*, Springer Dordrecht, **2nd edn** (2006), DOI:10.1007/1-4020-4133-0.

2 Kong X & Gosselin C, Type synthesis of parallel mechanisms, *Springer Tracts in Advanced Robotics*, **33** (2007), DOI: 10.1007/978-3-540-71990-8.

3 Merlet J P, Still a long way to go on the road for parallel mechanisms, *Proc ASME 2002 DETC Conf Montreal*, (2002).

4 Londhe P S, Singh Y, Santhakumar M, Patre B M &Waghmare L M, Robust nonlinear PID-like fuzzy logic control of a planar parallel (2PRP-PPR) manipulator, *ISA Trans,* **63** (2016) 218–232, DOI:10.1016/j.isatra.2016.02.016.

5 Nespoli A, Besseghini S, Pittaccio S, Villa E & Viscuso S, The High potential of shape memory alloys in developing miniature mechanical devices: A review on shape memory alloy mini-actuators, *Sensors and Actuat A- Phys*, **158(1)** (2010) 149–160, DOI:10.1016/j.sna.2009.12.020.

6 Raparelli T, Zobel P B & Durante F, Design of a parallel robot actuated by shape memory alloy wires, *Mater Trans*, **43** (2002) 1015–1022, DOI:10.2320/MATERTRANS.43.1015.

7 Khidir E A, Mohamed N A, Nor M J M & Mustafa M M, A new method for actuating parallel manipulators, *Sensors and Actuat A-Phys*, **147(2)** (2008) 593–599, DOI:10.1016/j.sna.2008.06.018.

8 Shi Z, Wang T, Liu D, Ma C & Yuan X, A fuzzy PID-controlled SMA actuator for a Two-DOF Joint, *Chinese J Aeronaut*, **27(2)** (2014) 453–460, DOI: 10.1016/j.cja.2014.02.015.

9 Nakshatharan S S, Dhanalakshmi K & Josephine S R D, Fuzzy-based sliding surface for shape memory alloy wire actuated classical super-articulated control system, *Appl Soft Comput*, **32** (2015) 580–589, DOI: 10.1016/j.asoc.2015.03.057.

10 Josephine S R D, Dhanalakshmi K & Nakshatharan S S, Bidirectional angular control of an integrated sensor/actuator shape memory alloy-based system, *Measurement*, **69** (2015) 210–221, DOI: 10.1016/j.measurement.2015.02.058.

11 Lambert T R, Gurley A & Beale D, SMA actuator material model with self-sensing and sliding-mode control; experiment and multibody dynamics model, *Smart Mater Struct*, **26(3)** (2017) 035004, DOI: 10.1088/1361-665X/aa5485.

12 Hadi A, Yousefi-Koma A, Moghaddam M M, Elahinia M & Ghazavi A, Developing a novel SMA-actuated robotic module, *Sensors and Actuat A-Phys*, **162(1)** (2010) 72–81, DOI: 10.1016/j.sna.2010.06.014.

13 Majima S, Kodama K & Hasegawa T, Modelling of shape memory alloy actuator and tracking control system with the model, *IEEE Trans Control Syst Technol*, **9(1)** (2001) 54–59, DOI: 10.1109/87.896745.

14 Nguyen B K & Ahn K, Feedforward control of shape memory alloy actuators using fuzzy-based inverse preisach model, *IEEE Trans Con Syst Technol*, **17(2)** (2009) 434–441, DOI: 10.1109/TCST.2008.924580.

15 Gorbet R B, Wang D W L & Morris K A, Preisach model identification of a two-wire SMA actuator, *Proc IEEE Int Conf Robot Autom*, (1998) 2161–2167, DOI: 10.1109/ROBOT.1998.680641.

16 Elahinia M H & Ashrafiuon H, Nonlinear control of a shape memory alloy actuated manipulator, *J Vib Acoust*, **124(4)** (2002) 566–575, DOI: 10.1115/1.1501285.

17 Dutta S M, Ghorbel F H & Dabney J B, Modelling and control of a shape memory alloy actuator, *Int Symp Intel Contr Limassol Cyprus*, (2005) 1007–1012, DOI: 10.1109/.2005.1467151.

18 Tai N T & Ahn K K, Adaptive proportional–integral–derivative tuning sliding mode control for a shape memory alloy actuator, *Smart Mater Struct*, **20(5)** (2011) 055010, DOI: 10.1088/0964-1726/20/5/055010.

19 Singh D, Choudhury R, Yogesh Singh & Mukherjee M, Workspace analysis of 3-DOF U-shape base planar parallel robotic motion stage using shape memory alloy restoration technique (SMART) linear actuators, *SN Appl Sci*, **3(511)** (2021) DOI: 10.1007/s42452-021-04490-y.

20 Orlando F, Joseph M & Podder T, Sliding mode control of a shape memory alloy actuated active flexible needle, *Robotica*, **36(8) (**2018) 1–18, DOI: 10.1017/S0263574718000334.

21 Ianagui A & Tannuri E A, A sliding mode torque and position controller for an antagonistic SMA actuator, *Mechatronics*, **30** (2015) 126–139, DOI: 10.1016/j.mechatronics.2015.06.010.

22 Wei W, Yunxi T & Li C, Controlling bending deformation of shape memory alloy-based soft planar gripper to grip deformable objects, *Int J Mech Sci*, **193** (2021) 106181, DOI: 10.1016/j.ijmecsci.2020.106181.

23 Hsia T C S, A new technique for robust control of servo systems, *IEEE Trans Ind Electron*, **36(1)** (1989) 1–7, DOI: 10.1109/41.20338.

24 Hsia T C S, Lasky T A & Guo Z, Robust independent joint controller design for industrial robot manipulators, *IEEE Trans Ind Electron*, **38(1)** (1991) 21–25, DOI: 10.1109/41.103479.

25 Jin M, Lee J, Chang P H & Choi C, Practical nonsingular terminal sliding-mode control of robot manipulators for high-accuracy tracking control, *IEEE Trans Ind Electron*, **56(9)** (2009) 3593–3600, DOI: 10.1109/TIE.2009.2024097.

26 Jin M, Lee J & Tsagarakis N G, Model-free robust adaptive control of humanoid robots with flexible joints, *IEEE Trans Ind Electron*, **64(2)** (2016) 1706–1715, DOI: 10.1109/TIE.2016.2588461.

27 Jin M, Lee J & Ahn K K, Continuous nonsingular terminal sliding-mode control of shape memory alloy actuators using time delay estimation, *IEEE/ASME Trans on Mechatronics*, **20(2)** (2015) 899–908, DOI: 10.1109/TMECH.2014.2323897.

28 Wang Y, Luo G, Gu L & Li X, Fractional-order nonsingular terminal sliding mode control of hydraulic manipulators using time delay estimation, *J Vib Control*, **22(19)** (2015) 3998–4011, DOI: 10.1177/1077546315569518.

29 Lee J, Jin M & Ahn K K, Precise tracking control of shape memory alloy actuator systems using hyperbolic tangential sliding mode control with time delay estimation, *Mechatronics*, **23(3)** (2013) 310–317, DOI: 10.1016/j.mechatronics.2013.01.005.

30 Young K D, Utkin V I & Ozguner U, A control engineer's guide to sliding mode control, *IEEE Trans Contr Syst Technol*, **7(3)** (1999) 328–342, DOI: 10.1109/87.761053.

31 Hung J Y, Gao W & Hung J C, Variable structure control: A Survey, *IEEE Trans Ind Electron*, **40(1)** (1993) 2–22, DOI: 10.1109/41.184817.

32 Patrick H, Meng W K, Tong H T &Joo K T, Kinematics analysis and mechatronics system design of a 3-DOF in-parallel actuated mechanism, *Seventh Int Conf Contr, Automat, Robotic Vision (ICARCV'O2)*, (2002) 950–955, DOI: 10.1109/ICARCV.2002.1238552.

33 Sadjadian H & Taghirad H D, Kinematic, singularity and stiffness analysis of the hydraulic shoulder: A 3-d.o.f. redundant parallel manipulator, *Adv Robot*, **20(7)** (2006) 763–781, DOI: 10.1163/156855306777681366.

34 Gosselin C & Angeles J, Singularity analysis of closed-loop kinematic chains, *IEEE Trans Robot Automat*, **6(3)** (1990) 281–290, DOI: 10.1109/70.56660.

35 Ranjith Pillai R & Ganesan M, Intelligent controller for robust orientation control of smart actuator-based parallel manipulator, *Proc Inst Mech Eng Part C J Mech Eng Sci*, **236(20)** (2022) 10573–10588, DOI: 10.1177/09544062221104022.

36 Ranjith Pillai R & Ganesan M, Modified PID like fuzzy servo control applied to smart actuator-based miniature parallel robot, *J Intell Fuzzy Syst*, **41(1)** (2021) 735–755, DOI: 10.3233/JIFS-202572.